


**AUTHOR QUERY FORM**

	<b>Journal:</b> AM  <b>Article Number:</b> 9669	<b>Please e-mail or fax your responses and any corrections to:</b>  <b>E-mail:</b> <a href="mailto:corrections.essd@elsevier.sps.co.in">corrections.essd@elsevier.sps.co.in</a>  <b>Fax:</b> +31 2048 52799
---	---	---

Dear Author,

Please check your proof carefully and mark all corrections at the appropriate place in the proof (e.g., by using on-screen annotation in the PDF file) or compile them in a separate list. Note: if you opt to annotate the file with software other than Adobe Reader then please also highlight the appropriate place in the PDF file. To ensure fast publication of your paper please return your corrections within 48 hours.

For correction or revision of any artwork, please consult <http://www.elsevier.com/artworkinstructions>.

Any queries or remarks that have arisen during the processing of your manuscript are listed below and highlighted by flags in the proof. Click on the 'Q' link to go to the location in the proof.

Location in article	Query / Remark: <a href="#">click on the Q link to go</a> Please insert your reply or correction at the corresponding line in the proof
<a href="#"><u>Q1</u></a>	Please confirm that given names and surnames have been identified correctly.
<a href="#"><u>Q2</u></a>	Please check whether the designated corresponding author address (B. Li) and telecommunication data (S.P. Joshi) correct, and amend if necessary.
<a href="#"><u>Q3</u></a>	Please update Ref. [36].

Thank you for your assistance.



# Rate-dependent hardening due to twinning in an ultrafine-grained magnesium alloy

Bin Li<sup>a,b,\*</sup>, Shailendra P. Joshi<sup>c,\*</sup>, O. Almagri<sup>d</sup>, Q. Ma<sup>a</sup>, K.T. Ramesh<sup>d</sup>, T. Mukai<sup>e</sup>

<sup>a</sup> Center for Advanced Vehicular Systems, Mississippi State University, Starkville, MS 39759, USA

<sup>b</sup> Center for Advanced Metallic and Ceramic Systems, Johns Hopkins University, Baltimore, MD 21218, USA

<sup>c</sup> Department of Mechanical Engineering, National University of Singapore, Singapore 117576, Singapore

<sup>d</sup> Department of Mechanical Engineering, Johns Hopkins University, Baltimore, MD 21218, USA

<sup>e</sup> National Institute of Materials Science, Sengen, Japan

Received 28 August 2011; received in revised form 1 December 2011; accepted 1 December 2011

## Abstract

An ultrafine-grained (UFG) ZK60 Mg alloy with an average grain size of  $\sim 1.0 \mu\text{m}$  was processed by extrusion at relatively low temperature (488 K) with a high area reduction ratio ( $\sim 25$ ). The mechanical behavior of the UFG Mg alloy is investigated over strain rates spanning nearly eight decades ( $10^{-4}$ – $10^4 \text{ s}^{-1}$ ). The stress–strain responses in the quasi-static ( $\sim 10^{-4} \text{ s}^{-1}$ ) and high rate ( $10^4 \text{ s}^{-1}$ ) regimes exhibit the characteristic sigmoidal profile that is a signature of  $\{10\bar{1}2\}\{10\bar{1}\bar{1}\}$  extension twinning. Further, this sigmoidal profile is accentuated at high rates, suggesting a rate effect of twinning induced hardening. X-ray diffraction (XRD) and analysis of the as-received and deformed microstructures indicate the occurrence of twinning even at the quasi-static rates of loading. This observation is contrary to some of the theoretical predictions that suggest suppression of twinning in Mg below critical grain sizes much larger than in the present work. From the XRD analysis we infer that the twin volume fraction increases with increasing applied strain rate. Transmission electron microscopy observations of the tested specimens reveal high density non-basal dislocations that may result from the activation of these slip systems following twinning-induced lattice reorientation.

© 2011 Acta Materialia Inc. Published by Elsevier Ltd. All rights reserved.

**Keywords:** Magnesium alloy; Ultrafine grained microstructure; Rate-dependent hardening; Twinning; Dislocations

## 1. Introduction

Magnesium and its alloys have attracted increasing attention in recent years because their low densities make these materials ideal for engineering applications in the automotive, aerospace and other industries. From the perspective of fuel efficiency these lightweight materials may significantly reduce the vehicle weight in potential structural applications. The attractiveness of Mg alloys as struc-

tural materials with impressive specific strength (strength/density) may possibly be realized through grain size refinement induced strengthening. However, the richness of the dynamics of deformation mechanisms, including dislocation slip and twinning, in this low symmetry hexagonal close-packed (hcp) crystal structure render its mechanical response vastly different from its high symmetry counterparts, e.g. face-centered cubic (fcc) metals. Owing to this, Mg alloys (and other hcp metals such as Ti and Zr) exhibit tension–compression asymmetry [1,2], strength anisotropy [1,2], high propensity to twinning [1,3,4] and a strong tendency for basal texture that strongly influences the mechanical properties [5]. These properties, which are closely related to defect processes, i.e. activation of multiple systems of dislocation slip (on the basal, prismatic and pyra-

\* Corresponding authors. Address: Center for Advanced Vehicular Systems, Mississippi State University, Starkville, MS 39759, USA (B. Li); tel.: +1 65 6516 4496; fax: +1 65 6779 1459 (S.P. Joshi).

E-mail addresses: binli@cavs.msstate.edu (B. Li), shailendra@nus.edu.sg (S.P. Joshi).

midal planes) and deformation twinning (on the first order and second order pyramidal planes), have attracted tremendous attention in recent studies aimed at improving the strength, ductility and workability of both coarse- and fine-grained Mg alloys.

As promising structural materials for a variety of applications (e.g. vehicles, armor for protection) the rate-dependent response of Mg alloys must be examined in order to understand their strengthening characteristics and resistance to failure over a wide range of loading rates. The strain rate dependence of the mechanical properties of Mg alloys has been studied in several previous reports [6–10]. At high loading rates Mukai and co-workers [6] reported high energy absorption and elongation to failure ( $\sim 20\%$ ) in a WE43 (Mg–Y–Nd–Zr) alloy, and increased strengthening and ductility in a fine-grained (grain size  $\sim 2\text{ }\mu\text{m}$ ) extruded ZK60 alloy compared with its coarse-grained counterpart [6]. More recently Tucker et al. [8] studied rate-dependent anisotropic effects on the strain rate dependence of a wrought AZ31B Mg alloy. They reported that the mechanical response in the rolling direction of the textured Mg alloy varied significantly when tested at strain rates of about  $10^{-3}\text{ s}^{-1}$  and  $10^3\text{ s}^{-1}$ . A similar but more complete study was conducted by Ulacia et al. [10] on an extruded AZ31B Mg alloy, in which the effects of temperature, loading direction and tension versus compression were exhaustively tested. These previous studies were performed on wrought Mg alloys with a grain size ranging from a few microns to a few tens of microns.

Ultrafine-grained (UFG) Mg alloys are of particular interest because grain refinement is an effective approach to achieve better mechanical properties. However, grain refinement may also mediate the already complicated interacting slip and twinning mechanisms in Mg. So far only limited studies have been carried out on UFG Mg alloys, especially with reference to their rate-dependent characteristics [9]. UFG materials can be fabricated by thermomechanical processes such as severe plastic deformation (SPD), where fine, dynamically recrystallized grains nucleate and grow when a large plastic strain is imposed on the materials [11–16]. In our recent work [9] a ZK60 alloy with a grain size of  $\sim 0.8\text{ }\mu\text{m}$ , processed by equal channel angular pressing (ECAP) was tested at quasi-static ( $\sim 10^{-3}\text{ s}^{-1}$ ) and high strain rates ( $\sim 10^3\text{ s}^{-1}$ ). We found that despite the small grain size its yield strength was close to that of its coarse-grained counterpart processed by conventional extrusion. Microstructural examination of that ECAP ZK60 alloy revealed over-aging and fragmentation of the precipitates (from elongated in the as-received materials to a spherical shape in the ECAP samples). This, together with texture changes due to ECAP [2], may have been responsible for the non-Hall–Petch mechanical behavior. This suggests that while some SPD processes may promote grain refinement in Mg, it may not necessarily result in strengthening if other important microstructural features are altered. In the UFG samples [9] sigmoidal (S-shaped) stress–strain responses were found at high strain rates, sug-

gesting that twinning may have occurred during deformation, despite the ultrafine grain size ( $0.8\text{ }\mu\text{m}$ ). Such a sharp increase in hardening rate has been considered the signature of  $\{10\bar{1}2\}\{10\bar{1}\bar{1}\}$  twinning in hcp metals [3], distinct from strain hardening in high symmetry crystal structures, which is dominated by dislocation interaction. Previous studies [17] show that the critical stress for twin nucleation is strongly dependent upon grain size and strain rate. Ghosh et al. [4] predicted that for Mg twinning should be suppressed when the grain size is reduced to below  $3.0\text{ }\mu\text{m}$ . Instead, dislocation slip and grain boundary mediated mechanisms dominate plastic deformation in the UFG regime.

Hence, several questions arise regarding the deformation behavior of UFG Mg alloys: (1) since high strain rates favor twinning in hcp metals [17] does twinning occur at quasi-static strain rates; (2) what are the controlling mechanisms of plastic deformation; (3) how does the loading rate influence twinning and the overall behavior? In this work we investigate the mechanical response of a UFG ZK60 (Mg–Zn–Zr) alloy and elucidate the underlying mechanisms through texture examinations by X-ray diffraction (XRD) and microstructural examination by transmission electron microscopy (TEM).

## 2. Experimental methods

A UFG ZK60 Mg alloy (grain size  $\sim 1.0\text{ }\mu\text{m}$ ) was processed via extrusion at a relatively low temperature of  $215^\circ\text{C}$  ( $488\text{ K}$ ) and a high area reduction ratio (ARR) of 25 (40 mm initial sample diameter reduced to 8 mm after extrusion). We then tested this extruded UFG alloy at quasi-static ( $\dot{\epsilon} \approx 10^{-4}\text{ s}^{-1}$ ) and high strain rates ( $\dot{\epsilon} \approx 10^3\text{--}10^4\text{ s}^{-1}$ ) and performed detailed TEM analyses on the specimens before and after high rate testing. Texture evolution was measured by XRD. For comparison, we also performed quasi-static ( $\dot{\epsilon} \approx 10^{-4}\text{ s}^{-1}$ ) micro-tension tests on the same material. Cylindrical samples were cut using wire electrical discharge machining (EDM) for quasi-static and high rate compression Kolsky bar tests [18] with the loading direction parallel to the extrusion direction. For quasi-static compression the specimen aspect ratio was maintained at  $\sim 1.5\text{--}2.0$ , while for the Kolsky bar tests an aspect ratio of 0.6 was used. The micro-tensile test specimens,  $1.7\text{ mm}$  long,  $500\text{ }\mu\text{m}$  wide and  $150\text{ }\mu\text{m}$  thick, were fabricated using a punching EDM technique [19].

Specimens for TEM were prepared from the as-extruded (untested) and tested samples for microstructural examination. The specimens were mechanically polished to  $\sim 130\text{ }\mu\text{m}$  thickness using a series of sandpapers down to 800 grit. Disks of  $3\text{ mm}$  diameter were then mechanically punched out of the polished samples and these disks were polished using a Tenupol-3 electropolisher with a perchloric acid ( $<2\%$ ) in ethanol solution. After electropolishing the specimens were cleaned by ion milling for  $\sim 0.5\text{ h}$  using gentle conditions of a low incident angle and a low voltage. Liquid nitrogen was applied during the ion mill-

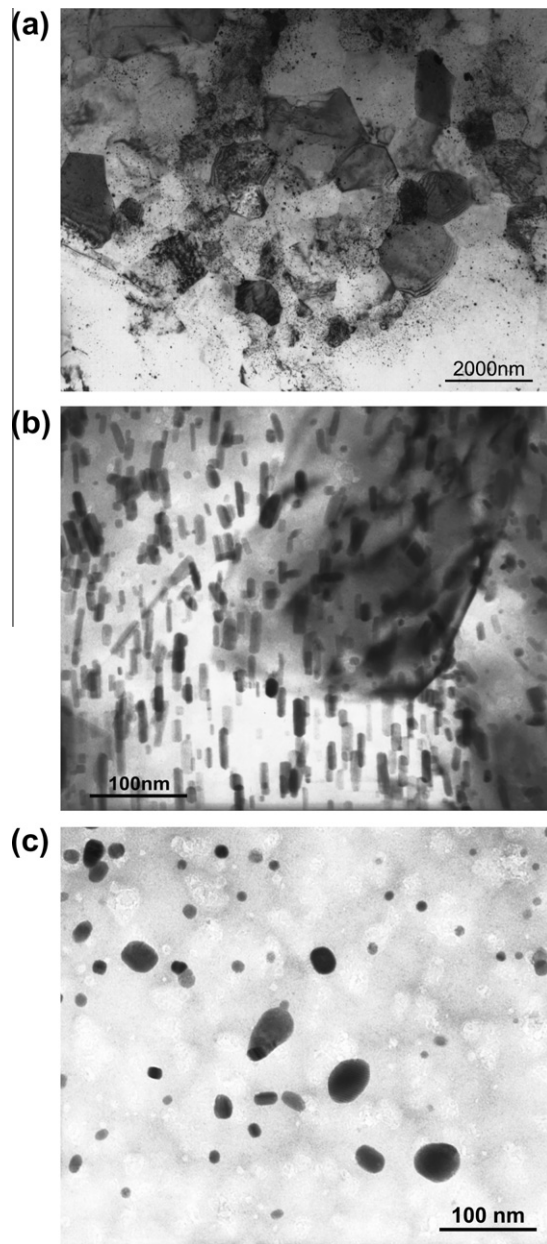


Fig. 1. (a) Grain structure of the extruded ZK60 magnesium alloy. The average grain size is about 1  $\mu\text{m}$ . (b) The majority of the precipitates are dispersed, rod-like in the ultrafine grains. (c) Besides the predominant rod-like precipitates, round particles are also observed.

ing. The electron-transparent specimens were examined using a Philips 420 microscope at an accelerating voltage of 120 keV.

### 3. Results and analysis

The microstructure of the as-extruded material is shown in Fig. 1a. The TEM micrograph shows that the average grain size is  $\sim 1.0 \mu\text{m}$ . This grain structure is more refined than materials extruded at higher temperatures (3.0–4.0  $\mu\text{m}$  or larger) [20]. It can also be seen that the microstructure contains very fine precipitates. As shown in Fig. 1b at higher magnification, these rod-like precipitates

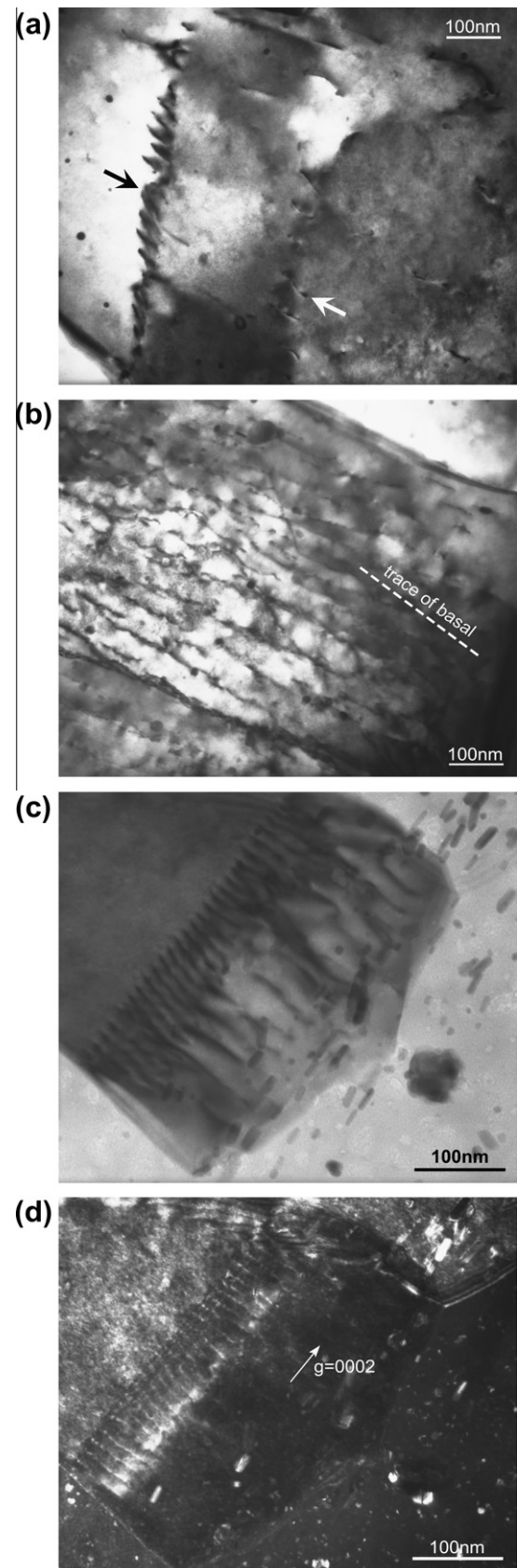


Fig. 2. Dislocation structures in the as-extruded UFG ZK60 alloy. (a) Dislocation pile-ups. (b) Dislocations arranged roughly parallel to the traces of the basal plane. (c and d) Contrast analysis shows that the dislocations in the pile-up in (c) are type  $\langle c \rangle$  dislocations with  $b = [0001]$ .



are aligned in a specific orientation. The precipitates in ZK60 alloys are  $\text{Mg}_2(\text{Zn,Zr})_3$ , and they have been well characterized previously [21–26]. Compared with the precipitates in the as-cast or ZK60 alloy extruded at higher temperatures [21] the aspect ratio of these precipitates is significantly smaller, probably because of the significant prior plastic work during extrusion. However, compared with our previous work on a ZK60 alloy produced by ECAP [9] the precipitates in the present extruded material still retain a relatively elongated shape (aspect ratio  $\sim 3.0$ – $4.0$ ), unlike the nearly spherical precipitates in the former. Besides the rod-like precipitates that predominate, round particles are also observed, but as a relatively small volume fraction, as shown in Fig. 1c.

### 3.1. TEM of as-extruded UFG Mg alloy

The dislocation structures in the as-extruded material were examined using TEM and are shown in Fig. 2. As expected, we observed various types of dislocation configurations created during the plastic work occurring during the extrusion process. Because the extrusion temperature is above the recrystallization temperature, dynamic recovery and recrystallization occurred during extrusion. Fig. 2a shows that dislocations are rearranged in pile-ups (indicated by the arrows), indicating that dynamic recovery occurred during extrusion. Fig. 2b shows that the dislocations are reorganized and aligned roughly parallel to the trace of the basal plane (marked with a dashed line). These are most likely basal dislocations with a Burgers vector  $1/3\langle 2\bar{1}10 \rangle$ . Basal dislocations can be activated most easily because the critical resolved shear stress (CRSS) is estimated to be nearly two orders of magnitude lower than that of non-basal dislocations [27]. In our observations the basal dislocations tend to be rearranged along the traces of the basal planes because during plastic deformation of a crystal the slip system with the maximum CRSS, i.e. the primary slip system, is activated first. Other slip systems may also be activated in order to satisfy the von Mises–Taylor criterion [28], but the most favored Burgers vector is predominant. If the crystal is properly oriented with respect to the electron beam the basal dislocations appear roughly parallel to the traces of the basal planes, as seen in Fig. 2b. However, such configurations of the basal dislocations can only be observed occasionally, indicating that basal slip, although with a low CRSS, cannot be the dominant deformation mechanism alone. The basal dislocations always appear like full dislocations or non-dissociated under conventional TEM, because according to atomistic simulations [29] the equilibrium split distance between the Shockley partial dislocations is only about 2–3 nm.

Fig. 2c and d shows another type of dislocation pile-up where the dislocations have a  $\langle c \rangle$  component. Fig. 2c is a bright field (BF) image, showing dislocations aligned across the whole grain. To identify the components of the Burgers vectors of the dislocations we performed weak

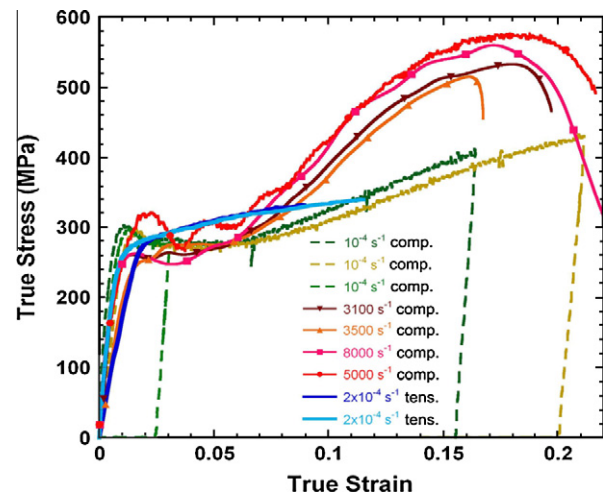


Fig. 3. Mechanical properties of the extruded ZK60 under tension (tens.) and compression (comp.) along the extrusion direction at various strain rates ranging from quasi-static to dynamic. The quasi-static compressions were unloaded and no failure occurred.

beam dark field (WBDF) imaging. WBDF is preferred to BF imaging when performing contrast analysis under two beam conditions, because of the presence of multiple Burgers vectors [21]. In Fig. 2d the dislocations were imaged by  $g(3g)$  WBDF, where  $g = 0002$ . The diffraction contrast clearly indicates that the dislocations have a  $\langle c \rangle$  component because the dislocations are visible under these specific diffraction conditions. Most of the dislocation pile-ups observed in our samples are of type  $\langle c \rangle$ . Under what conditions these type  $\langle c \rangle$  dislocations are produced and how they are reorganized during thermo-mechanical processing remains unknown. Meanwhile, type  $\langle a \rangle$  dislocations (both basal and prismatic) are invisible because  $g \cdot b = 0$ .

### 3.2. Macroscopic behavior

Fig. 3 shows the mechanical response of the UFG ZK60 alloy along the extrusion direction over a range of strain rates, from quasi-static ( $10^{-4} \text{ s}^{-1}$ ) to high strain rates (up to  $8 \times 10^3 \text{ s}^{-1}$ ). Tension and compression were conducted at quasi-static rates, but only compression tests were performed at high rates due to the limited sample volume. Except for quasi-static compression, all specimens were strained to failure. The compressive and tensile stress-strain responses of the UFG ZK60 alloy exhibit several salient features. (1) The compressive yield strength of this material is nearly rate-independent (the initial ripples in the high strain rate response are an artifact of the test rather than the material response). (2) The strain hardening behavior under high rate compression is significantly stronger than its corresponding quasi-static counterpart. (3) The quasi-static tensile yield strength is nearly equal to the compressive yield strength, but shows a qualitatively different hardening behavior than the compressive responses. In other words, the tension–compression asymmetry which is a commonly observed in Mg is not observed in this

UFG alloy. (4) The compressive responses along the extrusion direction present sigmoidal behavior, even at the quasi-static rates, and this behavior is more pronounced at high strain rates. Note that the yield and flow stresses in the present extruded UFG ZK60 alloy are higher compared with the ECAP counterpart with a similar grain size ( $0.8\ \mu\text{m}$ ) [9]. This may be partly attributed to retention of the rod-like precipitates (Fig. 1b) in the former, although texture may also play a role [14].

### 3.3. TEM of deformed UFG Mg alloy

Fig. 4 shows the TEM observations of the microstructure of the specimen tested at  $\dot{\epsilon} = 3.5 \times 10^3\ \text{s}^{-1}$ . Fig. 4a indicates that a high density of dislocations is produced during high rate compression and the dislocations are tangled. To analyze the nature of the Burgers vector of these dislocations, WBDF with  $g(3g)$  (where  $g = 2\bar{1}\bar{1}0$ ) was performed (Fig. 4b). With this  $g$  vector all the dislocations that have an  $\langle a \rangle$  component should be visible, but the  $\langle c \rangle = [0001]$  dislocations should be invisible. Indeed, as shown in Fig. 4b, a majority of these dislocations have an  $\langle a \rangle$  component. Note that under the diffraction conditions in Fig. 4b the electron beam is roughly parallel to the basal plane. Hence, the dislocations produced during plastic deformation (Fig. 4) are most likely non-basal and specifically on the prismatic planes. This is further substantiated by choosing  $g = 0002$  to image the dislocations (Fig. 4c) wherein most of the dislocations visible in Fig. 4b are now invisible, confirming that a majority of the dislocations generated at high strain rates are indeed of non-basal  $\langle a \rangle$  type. Finally, Fig. 4d shows another BF image of the dislocations indicating that some of them are aligned into a dislocation wall. It is worth noting that no well-defined stacking faults are observed in the as-extruded and deformed microstructures, which is significantly different from the wide stacking faults observed in coarse-grained, pure Mg deformed at room temperature [30]. The absence of wide stacking faults also confirms that the non-basal dislocations are indeed prismatic.

## 4. Discussion

The quasi-static compressive yield strength is much lower than its tensile counterpart in coarse-grained extruded Mg alloys when deformed along the extrusion direction, but the hardening rate in compression is significantly higher compared with the tensile hardening rate [2]. Both a lower yield strength and higher hardening rate in compression are attributed to extension twinning, the former due to a low CRSS and the latter induced by significant lattice reorientation and the interaction of extension twins with dislocations. On this backdrop it is interesting to note the lack of tension–compression asymmetry in the yield stress (Fig. 3) at quasi-static rates. This suggests that for this UFG Mg alloy compressive yielding might not be governed by extension twinning and non-basal slip may

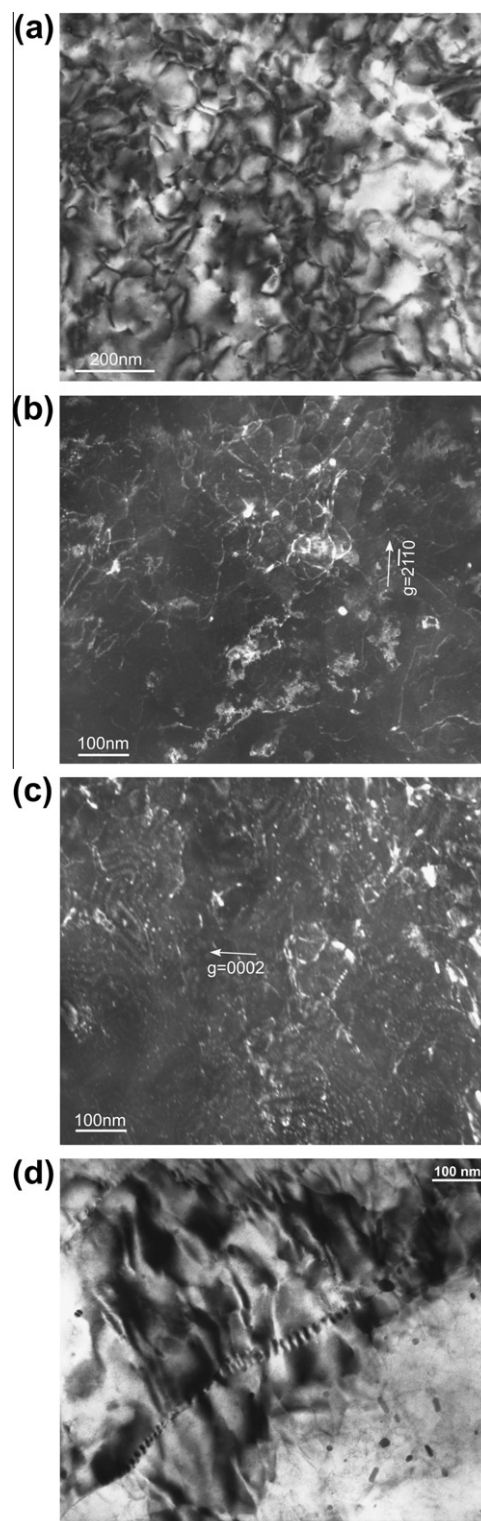


Fig. 4. (a) High density dislocations were produced during dynamic loading ( $\dot{\epsilon} = 3500\ \text{s}^{-1}$ ). (b) Dark field contrast analysis with a  $g(3g)$  weak beam shows that the majority of the dislocations have an  $\langle a \rangle$  component and are probably on the prismatic planes. (c) Choosing  $g = 0002$  to image the dislocations, most of the dislocations visible in (b) are now invisible, indicating that the majority of the dislocations generated at high strain rates are of non-basal  $\langle a \rangle$  type. (d) Another BF image of the dislocations indicating that some of them are aligned as a dislocation wall.

have a role to play, thereby raising the overall yield stress. The literature [4,17] also suggests that below a grain size of about  $3\ \mu\text{m}$  twinning may be superseded by dislocation slip. On the other hand, the same compressive response exhibits a sigmoidal shape, albeit milder than in coarse-grained Mg alloys [2], that is considered to be a signature of  $\{10\bar{1}2\}\{10\bar{1}\bar{1}\}$  extension twinning in hcp metals. These observations pose an interesting puzzle as to whether twinning has indeed occurred in the present case given the small grain size. To assess the likelihood of twinning in the quasi-statically deformed specimens we performed XRD measurements on the specimens before and after testing in order to examine the textural changes (Fig. 5). Fig. 5a shows the texture plot of the as-extruded sample. Despite the ultrafine grain size the pole figure presents the typical characteristic of extruded hcp metals where the basal planes are approximately parallel to the extrusion direction. However, the pole figures of the quasi-statically compressed specimen (Fig. 5b) signify a major change in that a strong basal pole appears that is at an angle of nearly  $90^\circ$

with reference to that of the as-extruded specimen (Fig. 5a), typical of  $\{10\bar{1}2\}\{10\bar{1}\bar{1}\}$  extension twinning. It is well understood that the as-extruded texture in Fig. 5a indicates that the majority of the grains are oriented such that their  $c$ -axes are aligned with the basal planes nearly parallel to extrusion direction, commonly referred to as basal texture. Consequently, compression along the extrusion direction results in  $c$ -axis extension in these grains, which favors tensile twinning. Under compressive strain this twinning mode reorients the basal planes from initially parallel to the extrusion direction to roughly perpendicular to the extrusion direction, such that elongation occurs in the direction perpendicular to the extrusion direction, accommodating the compressive strain [31]. The texture evolution in Fig. 5b indicates that some twinning must have occurred in the quasi-statically compressed UFG Mg alloy. This observation is at odds with the prediction that twinning should be suppressed below a grain size of  $\sim 3.0\ \mu\text{m}$  [4]. At a high rate ( $3.5 \times 10^3\ \text{s}^{-1}$ ) an even stronger basal pole (Fig. 5c) can be identified compared with that of the quasi-statically tested specimens, indicating that twinning is exacerbated at high rates.

Based on the XRD data, we calculated the twin volume fractions  $f_v$  in the as-extruded, quasi-statically tested and the dynamically tested specimens. In Fig. 6 the  $f_v$  values are obtained by incrementally integrating the diffraction intensity over the sample tilting angle  $\alpha$  (between  $0^\circ$  and  $90^\circ$ , i.e. from the center to the great circle of the pole figure) in the XRD at  $\alpha = 10.8^\circ$ ,  $19.8^\circ$  and  $38.3^\circ$  in the  $\{0001\}$  pole figure. At a given angle the samples tested at high strain rate possess the highest  $f_v$ , indicating that as the strain rate increases more deformation twins are activated in the ultrafine grains. This general trend is consistent with the enhanced hardening rate of the specimens deformed at high rates (Fig. 3). These results also support the phenomenological model proposed by Meyers et al. [17] for strain

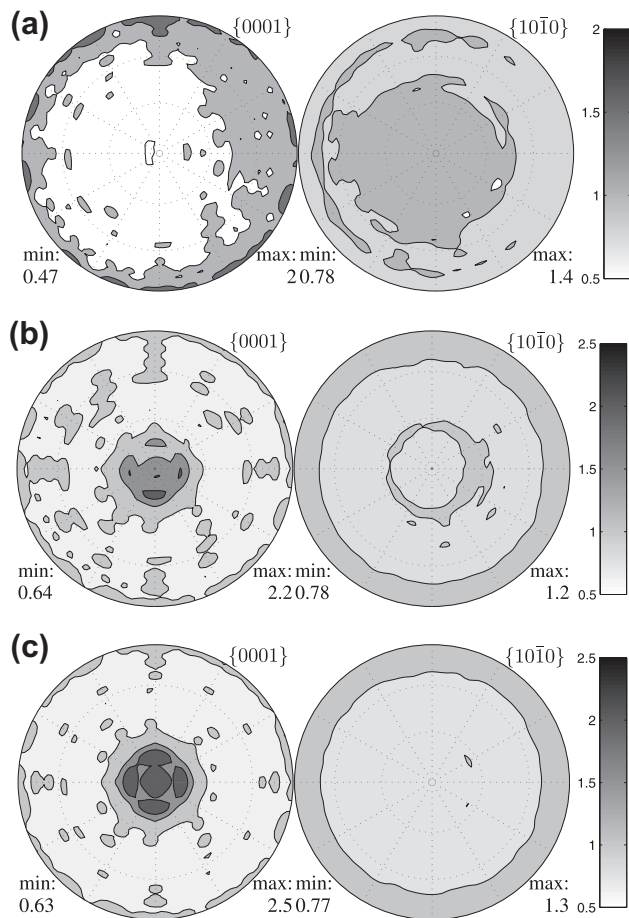


Fig. 5. Evolution of the texture at quasi-static and dynamic strain rates. (a) Pole figures of the as-extruded ZK60 alloy. (b) Pole figures of the sample deformed under compression at  $\dot{\epsilon} = 10^{-4}\ \text{s}^{-1}$  (see Fig. 3). A strong basal pole appears after deformation, indicative of  $\{10\bar{1}2\}\{10\bar{1}\bar{1}\}$  twinning. (c) Pole figures of the sample deformed at  $\dot{\epsilon} = 3500\ \text{s}^{-1}$ . The basal pole is stronger than that of the quasi-statically deformed sample. The extrusion direction is oriented out of the plane of the paper.

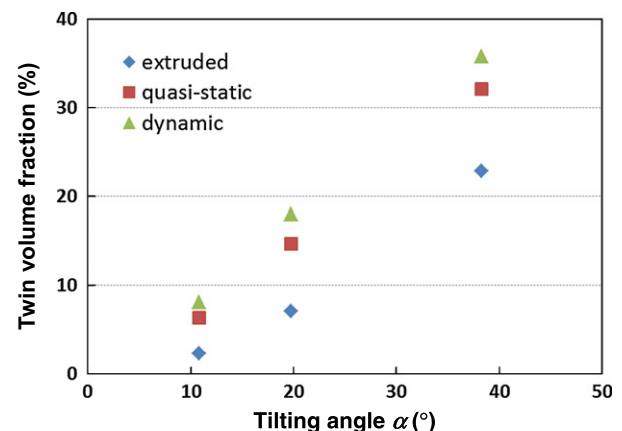


Fig. 6. Tension twin volume fraction as a function of the tilting angle  $\alpha$  of X-ray diffraction (XRD) in as-extruded, quasi-statically and dynamically deformed samples. The twin volume fraction was obtained by incremental integration of the basal pole figure intensity over  $\alpha$  at  $10.8^\circ$ ,  $19.8^\circ$  and  $38.3^\circ$ , respectively. At a given angle the dynamically tested sample has the highest twin volume fraction, consistent with the stress-strain responses (Fig. 3).



rate-dependent deformation twinning in hcp metals. Their model predicts that for small grain sizes slip is the dominant mode of deformation, but twinning may still be slightly favored at very high rates of loading, especially at room temperature. On this backdrop it is interesting that our UFG alloy exhibits some twinning even at a quasi-static strain rate.

It should be noted that while the flow behavior characteristics (Fig. 3) and texture analysis (Fig. 5) strongly indicate the occurrence of extension twinning, our TEM observations of the microstructures deformed at the quasi-static and high rates do not reveal well-defined twin boundaries (TB). We discuss this apparent anomaly through two arguments. Firstly, according to Barnett [32] the number of twins in each grain is a more appropriate measure than the twin volume fraction, especially at small grain sizes. Assuming a constant number of twins emitted by a unit area of grain boundary, Barnett inferred that the number of twins per grain should be proportional to  $d^2$  ( $d$  is the grain size) using a simplistic scaling rule. Although the area fraction of grain boundaries per unit volume increases as the grain size is reduced (i.e. is inversely proportional) and seemingly the decrease in grain size would generate a larger number of twins per unit volume, the number of grains per unit volume scales with  $d^3$ . Hence, on average, as the grain size is reduced the chances of finding deformation twins in each grain drop drastically. This scaling rule shows a trend that agrees with metallographic measurements. This inference may also demonstrate why deformation twins are rarely observed in fine-grained Mg, however, as shown in our experiments, this does not necessarily indicate that twinning cannot occur.

Another possible reason lies in the unique properties of  $\{10\bar{1}2\}\{10\bar{1}\bar{1}\}$  twinning. In a recent work [33] it was uncovered that, unlike other twinning modes in hcp,  $\{10\bar{1}2\}\{10\bar{1}\bar{1}\}$  involves no well-defined zonal twinning dislocations at the TB. Instead, conversion of the parent lattices to twin lattices can be achieved by local atomic shuffling where the basal planes of the parent are reconstructed into the prismatic planes of the twin and vice versa. Atomic shuffling for twinning in hcp metals was described in seminal works by Bilby and Crocker [34] and Christian and Mahajan [35]. The magnitude of local shuffling required for this lattice reconstruction is much smaller than any known matrix dislocations, resulting in a twinning mode with highly mobile TB and, probably, a low CRSS for twin nucleation and growth in coarse-grained Mg. The most recent high resolution TEM observations support this mechanism [36]: the actual TB of  $\{10\bar{1}2\}\{10\bar{1}\bar{1}\}$  twinning in Co and Mg can deviate entirely from the  $\{10\bar{1}2\}$  twinning plane with a magnitude greater than  $45^\circ$ . In other words, this most commonly observed twinning mode in hcp metals need not have a rigorously defined twinning plane, unlike other twinning modes. To our knowledge such a strikingly large deviation can only be rationalized by an atomic shuffling mechanism [32], rather than by twinning dislocations that are strictly

bounded in the twinning plane. Hence, it is likely that given such a fine grain size entire grains whose orientations favor twinning would undergo rapid reorientation, leaving few traces of observable TB, or the TB lose the sharp, planar morphology that is always observed in other twinning modes and become difficult to identify. In fact, Partridge and Robertson [37] observed abnormal TB migration in Mg at room temperature. In their optical microscopic observations the existing  $\{10\bar{1}2\}\{10\bar{1}\bar{1}\}$  TB evolved extreme incoherency under very small stresses produced by indentation. More recently Ma et al. [38] observed that dynamically recrystallized grains in an extruded Mg alloy satisfy the  $\{10\bar{1}2\}\{10\bar{1}\bar{1}\}$  twin orientation relationship, but the grain boundaries (TB) completely lose the regular, coherent and planar morphology. It is conceivable that in UFG microstructures such as the present one when twinning occurs in a given grain it may consume that grain entirely giving it a new orientation and leaving little forensic evidence of this process identifiable by TEM. Therefore, the rate-dependent kinetics of twinning in fine-grained Mg should be carefully investigated using controlled real and virtual experiments. Caution should be exercised when concluding that no twinning could occur in the ultrafine grain size range at quasi-static or lower strain rates. As seen in this work, twinning can still be activated in UFG Mg.

Mechanisms of hardening in the flow response have been extensively studied experimentally and by modeling, including activation of non-basal slip and compression twin modes following tensile twinning induced textural evolution [31], the Basinski mechanism [39] in which initially glissile matrix dislocations become trapped and sessile in twinned lattices because the orientations of the twins are less favorable for slip under the external load, the dislocation transmutation mechanism between the matrix and twins [40], which can be construed as a generalization of the Basinski mechanism, twin–twin interactions, and interactions between TB and matrix dislocations that impinge and deposit at the TB and hinder twin growth [41].

In the range of ultrafine grain sizes at quasi-static rates twinning becomes increasingly difficult in hcp metals as grain size decreases and higher stress is needed to activate twinning. Given that XRD shows evidence of twinning at quasi-static rates (Fig. 5b), we posit that twinning may already have occurred, albeit at a higher stress, when bulk yielding is reached. Following this, the mild strain hardening is likely due to the activation of non-basal slip, with some contribution from twinning. The dominant deformation mechanism is replaced by non-basal dislocation slip [3,4,10]. At high strain rates profuse twinning may have occurred in the fine grains as local (e.g. at grain boundaries) stresses may be high enough, as necessitated by the theories of size-dependent twinning [4,17], and a higher twin volume fraction is required to accommodate the plastic strain. The lattice reorientation resulting from twinning may lead to activation of plastically hard non-basal slip modes (Fig. 4) that further assist hardening, as in the case of coarse-grained Mg. The resulting enhanced hardening in



the UFG alloy at high rates compared with quasi-static rates may be a consequence of the above mentioned twinning induced hardening mechanisms. In addition, it may be possible that the fine precipitates ~~may~~ assist in work hardening by interacting with slipping and twinning [42,43]. Recently, Stanford et al. [44] and Robson et al. [45] discussed the effect of precipitate shape and distribution on the overall response and underlying deformation mechanisms. Their experiments and modeling indicated that twin–precipitate interaction could assist work hardening through a variety of mechanisms that include: the Orowan mechanism (twin dislocation–precipitate interaction), twin shape changes accommodated by slip within twins, back-stress arising from elastically deforming precipitates during twin growth, and secondary slip around the precipitates. In the context of the present results ~~it may be concluded~~ that these mechanisms could accentuate work hardening at high strain rates.

## 5. Conclusions

We processed a ZK60 Mg alloy by extrusion at a relatively low temperature (488 K) and with a high ARR of  $\sim 25$ . An ultrafine-grained microstructure with an average grain size of  $\sim 1.0 \mu\text{m}$  was obtained. TEM examinations show predominantly rod-like precipitates with an aspect ratio of 3.0–4.0. Round, over-aged particles were also observed. The UFG ZK60 alloy at quasi-static and high strain rates exhibits a higher yield strength compared with the coarse-grained ZK60 alloy, which is attributed to the small grains and retention of the rod-like precipitates.

At quasi-static rates compression–tension yield asymmetry is markedly absent. The stress–strain response still presents a sigmoidal behavior, which is a signature of the activation of  $\{10\bar{1}2\}\langle 10\bar{1}\bar{1}\rangle$  twinning. XRD measurements of the evolution of texture before and after deformation strongly indicate the presence of twinning as a mechanism, despite the small grain size and low strain rate. Contrary to some of the theoretical predictions that twinning would be suppressed when the grain size is reduced below  $3.0 \mu\text{m}$  our results indicate that twinning may still play an important role in plastic deformation of fine grains at low strain rates.

At high compressive strain rates a sharp increase in strain hardening is observed, indicative of the activation of profuse twinning. The twin volume fraction increases as the strain rate increases. The rate-dependent hardening behavior of the UFG Mg alloy is consistent with the model proposed by Meyers et al. [17]. TEM observations reveal a high density of non-basal dislocations in the deformed samples.

## Acknowledgements

This work was supported at the Center for Advanced Metallic and Ceramic Systems (CAMCS) sponsored by ARMAC-RTP, DAAD19-01-2-0003 and the US Army Re-

search Laboratory – Materials Center of Excellence (cooperative Agreement No. W911NF-06-2-0006). B.L. and Q.M. gratefully acknowledge support from the Center for Advanced Vehicular Systems, Mississippi State University. S.P.J. acknowledges partial financial support from the US Army International Technology Center, Pacific (ITC-PAC) through Research Contract No. FA5209-10-P-0047 (R-265-000-338-597).

## References

- [1] Avedesian MM, Baker H, editors. Magnesium and magnesium alloys. Materials Park, OH: ASM International; 1998.
- [2] Agnew SR, Horton JA, Lillo TM, Brown DW. Scripta Mater 2004;50:377–81.
- [3] Barnett MR, Keshavarz Z, Beer AG, Atwell D. Acta Mater 2004;52:5093–103.
- [4] Yang Q, Ghosh AK. Acta Mater 2006;54:5159–70.
- [5] Yapici GG, Karaman I. Mater Sci Eng A 2009;503:78–81.
- [6] Mukai T, Mohri T, Mabuchi M, Nakamura M, Ishikawa K, Higashi K. Scripta Mater 1998;39:1249–53.
- [7] Mukai T, Yamanoi M, Watanabe H, Ishikawa K, Higashi K. Mater Trans 2001;42:1177–81.
- [8] Tucker MT, Horstemeyer MF, Gullett PM, El Kadiri H, Whittington WH. Scripta Mater 2009;60:182–5.
- [9] Li B, Joshi SP, Azevedo K, Ma E, Ramesh KT, Figueiredo RB, et al. Mater Sci Eng A 2009; 517: 24–9.
- [10] Ulacia I, Dudamel NV, Galvez F, Yi S, Perez-Prado MT, Hurtado I. Acta Mater 2010;58:2988–98.
- [11] Valiev RZ, Islamgaliev RK, Alexandrov IV. Prog Mater Sci 2000;45:103–89.
- [12] Valiev RZ, Langdon TG. Prog Mater Sci 2006;51:881–981.
- [13] Figueiredo RB, Langdon TG. Mater Sci Eng A 2009;501:105–14.
- [14] Yamashita A, Horita Z, Langdon TG. Mater Sci Eng A 2001;300:142–7.
- [15] Horita Z, Matsubara Z, Makii K, Langdon TG. Scripta Mater 2002;47:255–60.
- [16] Matsubara K, Miyahara Y, Horita Z, Langdon TG. Acta Mater 2003;51:3073–84.
- [17] Meyers MA, Vöhringer O, Lubarda VA. Acta Mater 2001;49:4025–39.
- [18] Kolsky H. Proc Phys Soc London B 1949;62:676–700.
- [19] Joshi SP, Eberl C, Cao B, Ramesh KT, Hemker KJ. Exp Mech 2009;49:207–18.
- [20] Li B, Ma E, Ramesh KT. Metall Mater Trans A 2008;39:2607–14.
- [21] Clark JB. Acta Metall 1965;13:1281–9.
- [22] Mima G, Tanaka Y. Trans Jpn Inst Metals 1971;12:71–5.
- [23] Mima G, Tanaka Y. Trans Jpn Inst Metals 1971;12:76–81.
- [24] Mima G, Tanaka Y. Trans Jpn Inst Metals 1971;12:323–8.
- [25] Wei LY, Dunlop GL, Westengen H. Metall Mater Trans A 1995;26:1705–16.
- [26] Watanabe H, Moriawaki K, Mukai T, Ohsuna T, Hiraga K, Higashi K. Mater Trans 2003;44:775–81.
- [27] Obara T, Yoshinaga H, Morozumi A. Acta Metall 1973;21:845–53.
- [28] Taylor GI. J Inst Metal 1938;62:307–24.
- [29] Yasi JA, Hector LG, Trinkle DR. Acta Mater 2010;58:5704–13.
- [30] Li B, Yan MF, Sui ML, Ma E. Acta Mater 2009;57:173–9.
- [31] Kelley EW, Hosford WF. The plastic deformation of magnesium: technical report; 1967.
- [32] Barnett MR. Scripta Mater 2008;59:696–8.
- [33] Li B, Ma E. Phys Rev Lett 2009;103:035503.
- [34] Bilby BA, Crocker AG. Proc Roy Soc A 1965;288:240–55.
- [35] Christian JW, Mahajan S. Prog Mater Sci 1995;39:1–157.
- [36] Li B, Zhang XY, El Kadiri H, Wu X, Zhu YT, Ma Q, et al. Phys Rev Lett, submitted for publication.
- [37] Prtridge PG, Roberts E. Acta Metall 1964; 12: 1205–10.

- 606 [38] Ma Q, Li B, Marin EB, Horstemeyer MF. *Scripta Mater* 2011;65:823–6. 612
- 607 613
- 608 [39] Basinski ZS, Szczerba MS, Niewczas M, Embury JD, Basinski SJ. 614
- 609 *Rev Metall* 1997;94:1037–43. 615
- 610 [40] El Kadiri H, Oppedal AL. *J Mech Phys Solids* 2010;58:613–24. 616
- 611 [41] Li B, Ma E. *Acta Mater* 2009;57:1734–43. 617
- [42] Clark JB. *Acta Metall* 1968;16:141–52.
- [43] Gharghoury MA. *Philos Mag A* 1998;78:1137–49.
- [44] Stanford N, Geng J, Chun YB, Davies CHJ, Nie JF, Barnett MR. *Acta Mater* 2012;60:218–28.
- [45] Robson JD, Stanford N, Barnett MR. *Acta Mater* 2011;59:1945–56.